

University of Magdeburg
Faculty of Computer Science
Department of Simulation and Graphics



Bachelor Thesis

**Comparison of Vortex Extraction Methods in
the context of Simulated Blood Flow in
Cerebral Aneurysms**

Author

Raphael Badel

Supervisors

Prof. Dr.-Ing. Bernhard Preim

Dr.-Ing. Steffen Oeltze-Jafra

(Department of Simulation and Graphics)

Priv.-Doz. Dr.-Ing. Gabor Janiga

(Institute of Fluid Dynamics and Thermodynamics)

March 14, 2016

Declaration of Authorship

I hereby declare that this thesis has been composed by me and is based on my own work, unless stated otherwise. No other person's work has been used without due acknowledgement in this thesis. All references and verbatim extracts have been quoted, and all sources of information have been specifically acknowledged.

Date:

Signature:

Contents

1	Introduction	1
1.1	Scope of Thesis	3
1.2	Notations	5
2	Theory	7
2.1	Features	7
2.1.1	Well-Defined Features	8
2.2	Critical Points	8
2.2.1	Classification of Critical Points	9
2.3	Vortices	9
2.3.1	Informal Vortex Definitions	9
2.3.2	Vortex Core Region	10
2.3.3	Vortex Core Line	14
2.4	Embedded Vortices	15
3	Methods	17
3.1	Parallel Vectors Operator	17
3.1.1	Categories of Line Features	18
3.1.2	Compute Vector Fields	20
3.1.3	Compute Locations	23
3.1.4	Apply Selection Criteria	25
3.1.5	Construct Polylines	26
3.1.6	Filter Polylines	27
3.2	Angle Criteria	27
3.2.1	New Criterion	31
3.3	Post-Processing	32
4	Comparison	33
4.1	Qualitative Comparison	34
4.2	Quantitative Comparison	36
4.3	Results	38
5	Discussion	45
5.1	Outlook	47

Chapter 1

Introduction

Numerical simulations are carried out for many purposes, such as industrial processes or medical issues. It is the task of physical and engineering sciences to determine the necessary parameters and find corresponding boundary conditions to design a model that fits the dynamics of the underlying application. At present, this is frequently done for computational fluid dynamics (CFD) simulations of cerebral blood flow giving insights into its hemodynamics. This interest refers to cardiovascular diseases as a dominating cause of death. Among cardiovascular diseases, subarachnoid bleedings show a high mortality rate (28-day case fatality rate of 42% [17]) and can be ascribed to ruptured intracranial aneurysms in the majority of cases.

Intracranial Aneurysms An intracranial or cerebral aneurysm is a permanent balloon-like dilation of a cerebral blood vessel. In 80–90%, their morphology can be characterised by an aneurysm *sac* that clearly distinguishes from the actual vessel [44]. The transition region is called the *neck* [23].

Epidemiologic studies concerning the occurrence of cerebral aneurysms vary due to a laborious acquisition of data and time-dependent stages of the disorder [44]. The prevalence in the general population ranges from 2.3% [31] to 3.2% [43] and up to 3.6–6% [45].

To prevent a cerebral aneurysm from rupturing, different treatments are current practice. The clipping approach benefits from the common presence of a neck region and aims at blocking the inflow by the placement of a metal *clip*. In contrast, a *coil* that is placed inside the sac is supposed to reduce the aneurysmal velocity and thereby support blood clotting. The coagulation

should close the sac eventually and restore an unimpeded flow. A *stent* has the same purpose, but works as a stabiliser for the vessel. Its close-meshed boundary surface is intended to hamper and to divert the blood flow such that its majority does not enter the aneurysm sac.

Despite the rupture risk, the intervention involves a high risk itself. As a consequence, a general treatment of intracranial aneurysms should be avoided. Instead, the rupture potential can be assessed by considering suitable influencing factors [44].

Influencing Factors Among hemodynamic parameters of cerebral aneurysms, vortical flow patterns are qualitative parameters of special interest. In a study of 210 aneurysms, Cebal et al. [7] linked complex flow patterns to the rupture of aneurysmal walls. The authors refer to *complex* as “flow patterns that exhibit flow divisions or separations [...] and contain more than one [...] vortex structure” [6]. The occurrence of a single vortex is referred to as a *simple* pattern. In another study involving 119 aneurysms, Xiang et al. [48] confirm the significance of simple and complex flow patterns.

From a medical point of view, the detection and evaluation of vortices can contribute to the assessment of whether an aneurysm is treated or not.

Blood Flow Simulations To examine the blood flow in cerebral aneurysms, numerical simulations of the Navier-Stokes equations that assume blood as an incompressible Newtonian fluid are performed [11]. These simulations are based on patient-specific vessel and aneurysm geometries that are processed in a workflow pipeline as explained in detail by [11]. According to the author, the first four steps that form the basis of the blood flow simulations can be outlined as follows:

1. Patient-specific image acquisition of the vascular system of interest
2. Reliable vessel segmentation of all necessary vascular sections
3. Vessel *surface* reconstruction and its geometric processing to obtain high-quality surface meshes and anatomical landmarks
4. *Volume* grid generation based on a surface mesh to establish a numerical grid for the simulation

Having isolated the vessel surface, the simulations can especially consider the subsequent fluid-structure interactions [44], meaning the interaction of a deformable structure (surface) with an internal fluid flow (volume). The general necessary partition of the volume in finite compartments results in a set of nodes, edges, faces and cells. Depending on the topology, these sets are referred to as *structured* or *unstructured grids*. The former is based on a regular topology entailing a systematic indexing of elements. While the regular structure allows for efficient computations, it is not suitable for complex geometries that partly require adaptive grid sections. Unstructured grids feature exactly this flexibility by allowing an arbitrary topology of grid elements as well as varying cell forms.

The Navier-Stokes equations include partial derivatives that, by definition, assume the domain as a continuum. In a numerical solution process, this model transitions into discrete grid points that hold values of the domain [44]. The discretisation process distinguishes finite-difference methods (FDM), finite-volume methods (FVM) and finite-element methods (FEM).

Feature-Based Visualisation Due to the large amount of data arising from high-resolution numerical simulations, a manual investigation with direct visualisation techniques is tedious, time consuming and inaccurate. Instead, to automate parts of the analysis that are mostly not parametrised is favourable. The purpose of feature-based visualisations or feature-based algorithms is to reduce the amount of data to a smaller size by automatically extracting features. In the context of aneurysm diagnosis by means of vortices, a feature-based algorithm fits to the mental work flow, since researchers know beforehand what kind of feature they are looking for in the data.

1.1 Scope of Thesis

The definition of vortices as well as their extraction is a research area that is extensively and continuously discussed by a vast number of publications. The intense scholarly interest is attributable to vortices being a complex field of research that involves many physical and geometric quantities. Furthermore, vortices are in general unsteady features, which means that measured values can also vary over time. As a result, there are many approaches regarding the definition of a vortex. Popular studies distinguish core regions and core lines of

a vortex, whereas others do or do not consider the unsteady aspect. In some cases, various algorithms try to map the same definition.

Despite the numerous studies, there is no evidence of how to define a vortex in a generally valid manner down to the present day. Due to different fields of applications and datasets, that result from a variety of simulations, different algorithms show varying strengths and weaknesses. In the particular domain of intracranial aneurysms, recent studies [6, 26] examined vortices based on a steady view and vortex core lines.

As a consequence, this thesis involves a comparison of six vortex core line definitions [1, 22, 24, 34, 41, 42] that are restricted to steady simulations respectively to a single timestep of unsteady simulations. Since the implementation is based on the *Parallel Vectors Operator* [28], it can be applied to unstructured grids. The comparison features practical datasets that explicitly make use of this grid type.

The comparison is divided in a *qualitative* and a *quantitative* part. The qualitative part considers the number of vortices, their types based on critical points and to which extent vortices are found completely (by continuous core lines) or incompletely (by fragmented or too short lines). The quantitative part estimates the amount of false positives based on post-processing steps proposed in this thesis.

The outcome of this thesis attempts to find the best vortex core line definition for the given context. Moreover, the question is answered whether and, if so, which fixed combinations of definitions produce core lines in close proximity and hence, which vortices are captured. In other words: Would it be possible to produce a comprehensive result if a set of interpolated streamlines is computed from the outputs of several individual definitions approximating their behaviour? In the context of vortex core *regions* a similar approach is proposed by Biwas et al. [3].

The one or the other attempt aims at finding a set of core lines that is the best possible, in order that it can be used for advanced analysis or visualisation techniques: The already mentioned classification of simple and complex flow patterns [7] is based on the number of vortices as well as on streamlines that are integrated from core lines. In particular, Byrne et al. [6] quantitate the complexity of blood flow by the length of the core lines which makes accurate lines essential. In a paper on the detection of embedded vortices (see section 2.4),

Oeltze et al. [26] examine critical points along core lines. Although the authors propose own pre-processing steps to connect fragmented lines, the underlying concept relies on continuous lines that span the entire vortex nevertheless.

1.2 Notations

In the context of this thesis, vectors have the dimension of three as well as matrices being 3-by-3 square matrices. To differentiate them from scalar values, their variables are printed **bold**. Moreover, matrices use capital letters as variable names. The following symbols appear consistently throughout the next chapters:

\boldsymbol{v} : velocity

$\nabla\boldsymbol{v}$: velocity gradient/Jacobian

$\boldsymbol{\omega}$: vorticity

Chapter 2

Theory

The purpose of this chapter is to introduce vortices in the sense of a feature that can be extracted by a feature-based algorithm. Formal aspects are explained based on general properties of features as well as by taking the example of critical points. In the course of this chapter, vortex definitions are distinguished by their representation. Moreover, embedded vortices are introduced.

2.1 Features

“In the field of feature-based visualization, there is no formal definition of a feature in general” [33]. Intuitively, one would call any structure or pattern of interest in the data a ‘feature’ [19, 33].

In the context of spatial data, these patterns are geometric objects. This implies the first property of a feature: its *localizability* [33]. Consequently, the location in turn implies the *dimensionality* [33]. A set of locations, which is a set of single points, may belong to a feature of higher dimension such as a line, a surface or a region. Therefore, a feature can be classified into being a point feature (0D), a line feature (1D), a surface feature (2D) or a region feature (3D). The mentioned properties are essential, meaning that a feature needs them to exist. Depending on the kind of feature, there are further properties such as its *physical extent* (length, area, volume), *shape*, *strength* or *energy* [19].

2.1.1 Well-Defined Features

A feature is well-defined, if there is a mathematical definition for it that can be applied to a dataset in order to extract the feature [19, 46]. A well-known example for features of this kind are critical points.

From the existence of a definition, further properties, like *Galilean invariance*, arise. This property can be explained by the metaphor of an ‘ideal’ train, moving with constant speed in a relative uniform motion. Any experiment carried out on the moving train would produce the same results as in a stationary environment. In the context of velocity fields, this property implies that a feature does not change after a constant is added to the field. A definition based on quantities that do not directly depend on the velocity (velocity jacobian, its invariants, λ_2 , vorticity) is Galilean invariant. With the occurrence of velocity or a directly dependent quantity, a definition loses this property.

The mathematical definition also determines the *locality* of data, the feature depends on. According to [19] and [33], a definition is called local, if the feature only depends on quantities in a small neighbourhood around its locations. If these quantities in turn could be anywhere in the domain, the definition is called global. For example, a definition that is based on a certain streamline behaviour is global, since a streamline can potentially reach every point in the domain.

2.2 Critical Points

A critical point is a very basic feature and, in the context of vector field topology, helps to partition the flow field into regions of characteristic flow [37]. Such a point can be understood as a degenerated streamline [33]. Thus, a streamline that integrates into a critical point ends, because the streamline slope is indeterminate at this point [9].

A *critical point* is defined as the location \mathbf{x} where the vector field \mathbf{v} is zero.

$$\mathbf{v}(\mathbf{x}) = \mathbf{0} \tag{2.1}$$

This point is called an *isolated critical point*, if, in addition, the vector field in

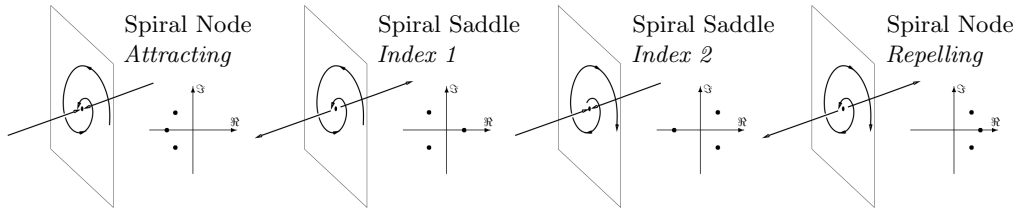


Figure 2.1: Stream line patterns near critical points and eigenvalue plane for spiralling flow. Illustration adapted from [14].

a small neighbourhood ε around it is defined [46].

$$\mathbf{v}(\mathbf{x} \pm \varepsilon) \neq \mathbf{0} \quad (2.2)$$

2.2.1 Classification of Critical Points

According to critical point theory (also known as the ‘phase-plane’ or ‘phase-space’ theory [29]) a critical point of first order can be classified by an eigenanalysis of $\nabla \mathbf{v}$ [46]. This classification refers to the patterns of nearby streamlines [15]. A complete and detailed overview of critical points and their flow patterns in 3D is given by Chong et al. [9].

Of special interest for vortical flow are critical points of a spiraling type (see Figure 2.1). They have in common that the eigenanalysis of $\nabla \mathbf{v}$ yields a single real eigenvalue and a pair of complex conjugate eigenvalues. The plane on which the flow spirals is defined by the complex pair [14].

2.3 Vortices

As well as critical points, vortices are features that can occur in vector fields. However, there is no agreement on their formal definition [33].

2.3.1 Informal Vortex Definitions

An informal definition, which probably reflects one’s intuition, is given by Roth [33]:

Everybody has an intuitive conception of a vortex and typically imagines something like a tornado.

Lugt [25] defines a vortex as

the rotating motion of a multitude of material particles around a common center.

Another definition was given by Robinson [32]:

A vortex exists when instantaneous streamlines mapped onto a plane normal to the vortex core exhibit a roughly circular or spiral pattern, when viewed from a reference frame moving with the center of the vortex core.

Byrne [4] describes the tornado metaphor on a more formal basis:

If you are unlucky enough to be hit by a hurricane you will experience the following. The wind will gradually increase to a ferocious velocity until you pass into the eye of the hurricane. The wind velocity will suddenly drop, and as the eye passes over you the velocity will drop to zero. After the center of the hurricane passes you the velocity will gradually increase until you pass out of the eye, when the wind will suddenly start howling again. The same thing happens with a tornado, but it is far more dangerous to observe this phenomenon.

In the past decades, researchers tried to translate these or similar ideas into mathematical definitions and algorithms. With the exception of a few publications [30, 35], most studies define the *core* of a vortex. These again can be divided into region-based and line-based representations.

2.3.2 Vortex Core Region

A vortex core region is based on the isosurface of a scalar field [21, 38] evaluated on grid nodes as shown in Figure 2.2a. For instance, thresholds on pressure, vorticity magnitude or helicity result in spatial regions of vorticity-like behaviour [13]. Advanced definitions are mostly based on $\nabla\mathbf{v}$ or its decomposition into its symmetric part \mathbf{S} and antisymmetric part $\mathbf{\Omega}$. These last-named values can also be evaluated on grid cells [19], because the velocity gradient is linear on tetrahedron elements, which are the basic modules for volume cells [14]. Grid node based regions, respectively isosurfaces, may appear smoother due

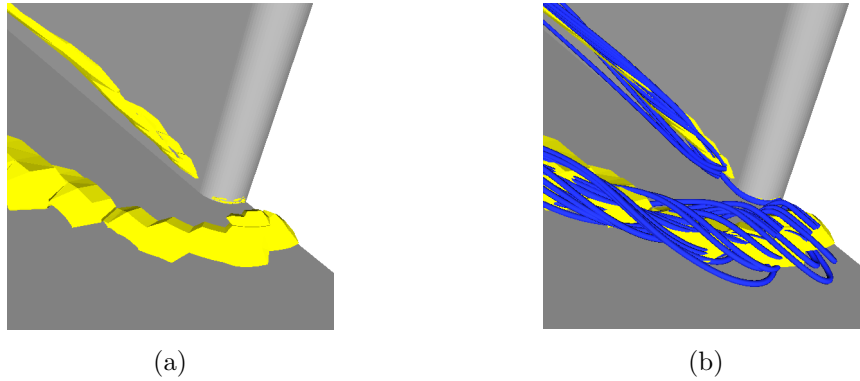


Figure 2.2: (a) Vortex cores defined by isosurfaces. In (b), streamlines are integrated from seedpoints within the interior. Images taken from [19].

to the procedure of the marching cubes algorithm. On the other hand, this procedure could produce surface fitting errors while grid cell based regions represent the core region accurately [19].

Complex Eigenvalues of Jacobian The same basic idea, that leads to a classification of critical points in section 2.2.1, is used in the Δ criterion by Chong et al. [9]. Spiraling flow, which was common to all above-mentioned critical points, can be verified at an *arbitrary* point in the domain. A vortex is defined as the regions, where $\nabla\mathbf{v}$ has a complex conjugate pair of eigenvalues. The characteristic equation for $\nabla\mathbf{v}$ is given by

$$\lambda^3 + P\lambda^2 + Q\lambda + R = 0. \quad (2.3)$$

where P , Q and R are the invariants of $\nabla\mathbf{v}$. In the case of incompressible flow, with $P = 0$, the discriminant Δ can be expressed as

$$\Delta = \left(\frac{1}{2}R\right)^2 + \left(\frac{1}{3}Q\right)^3. \quad (2.4)$$

To verify a complex conjugate pair of eigenvalues, it is sufficient to check for a positive Δ . Due to different definitions for the discriminant in the literature, a complex pair may have the opposite sign. The derivation of the discriminant based on *Cardano's Formula*, as stated in [33], considers compressible flow as well and simplifies to (2.4) in the incompressible case. In another step, eigenvalues can be computed directly.

Swirl Parameter Berdahl and Thompson [2] extend the Δ criterion and introduce the *swirl parameter* τ . This parameter tells how much a fluid particle that convects through spiraling flow is captured by the swirl. Given a threshold, the authors define a vortex as regions of a complex conjugate pair of eigenvalues in combination with a certain impact of swirling motion to a particle.

Swirling Strength Zhou et al. [50] extend the Δ criterion as well. They define the imaginary part of the complex conjugate pair of eigenvalues as the *swirling strength*. Since this value is signed, they suggest to use the *squared swirling strength*, which is analogous to *enstrophy* (squared magnitude of vorticity [1]) and thereby dimensionally consistent. A threshold subsequently filters out regions of strong swirling motion.

In [37] and [39], the authors define *vortex strength* respectively *rotations strength* in the same manner as swirling strength, but reference Chong et al. [9] as their source, which I, to the best of my knowledge, cannot confirm. Instead, Zhou et al. should be referenced. Chong et al. [9] name a *rate of spiral*, which they define as $\frac{\sigma}{\omega}$, where σ is the real part and ω the positive imaginary part of the complex conjugate pair. This idea was later continued by Chakraborty et al. [8].

Positive Second Invariant of Jacobian The second invariant of a general matrix, Q , is given by

$$Q = \frac{1}{2}(\|\boldsymbol{\Omega}\|^2 - \|\boldsymbol{S}\|^2). \quad (2.5)$$

The Q criterion by Hunt et al. [16] identifies the vortex core as regions, where the second invariant of $\nabla\boldsymbol{v}$ is positive. Additionally, the pressure has to reach a minimum in that region. Jeong and Hussian [18] state, that the second condition is true in most situations when the first one is true, although this cannot be guaranteed.

A positive Q means a domination of the absolute vorticity magnitude over the absolute strain rate and vice versa [10, 37, 50].

In the context of incompressible flow, the Okubo-Weiss criterion [27, 47] is identical to the Q criterion [37].

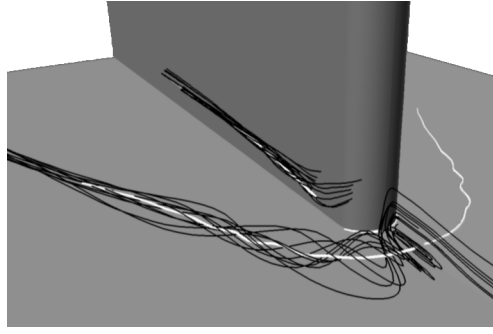


Figure 2.3: A vortex core line (white) with streamlines (black) spiralling around the core. Image taken from [19].

Lambda2 (λ_2) Jeong and Hussian [18] present an improved version of the Q criterion. According to the authors “ Q can also be interpreted as the source term of pressure” [18]. After deriving the pressure Hessian from the Navier-Stokes equations, they define a symmetric matrix as $\mathbf{S}^2 + \mathbf{\Omega}^2$. In contrast to Q , this matrix neglects two unwanted effects: Unsteady irrotational straining and viscosity [18].

The authors define a vortex core as a connected region where $\mathbf{S}^2 + \mathbf{\Omega}^2$ has two negative eigenvalues. The title λ_2 refers to an ascending sorting of the eigenvalues.

Shortcomings of Region Definitions A known disadvantage of vortex core *regions* is that they cannot distinguish between different vortices in close proximity [19], even if they have a different sense of rotation [33]. This is attributable to the fundamental assumption that a vortex core region is the uniform interior of a boundary surface. Another disadvantage is that this boundary surface depends on a threshold, given that the chosen definition includes one. But even if a definition is parameter free, the field of application may require further thresholds on intuitive values like vorticity magnitude or helicity to eliminate false positives [36, 37, 50]. In conclusion, the extent of the boundary surface, and thereby the extent of the vortex core region, is hard to define [33].

2.3.3 Vortex Core Line

Another way of representing a vortex core is by a *line*. It follows the intuitive concept of a “center line of the swirling flow structure, around which the flow spirals” [33]. A centerline, as shown in Figure 2.3, brings several advantages over regions. First of all, vortex core lines can differentiate between vortices that are in close proximity [33]. Furthermore, a line is a 1D feature and therefore it only has an extent in one dimension. The extent in other dimensions is infinitesimal and hence, no boundary, as with regions, has to be defined. Although the extraction of lines can generally depend on parameters, this may lead to more robust solutions [33].

The main disadvantage of line definitions is the computational complexity [21]. Additionally, in special cases, when the center of swirling flow is an extensive region of constant flow, line definitions could produce many individual lines that actually belong to one single core [21, 33].

The representation as a centerline is common to all following definitions. What differs is the understanding of what the center is [37].

Streamlines from Critical Points Globus et al. [12] suggest to represent the center as a streamline that originates from a critical point [49]. Yates et al. [49] add to demand minimal curvature along the streamline. They also discuss the study of Levy et al. [24], in which the authors state that a streamline, that is integrated from an extremum of normalized helicity, will eventually converge to a critical point.

The underlying assumption of these studies is that a critical point can make predictions on streamline characteristics and vice versa. As critical points, being a local feature, and streamlines, being a global feature, there is no reliable fundament for that assumption [33]. However, Roth [33] states that “for well-formed vortices the core is often close to a streamline”. The author implicitly as well as the above-mentioned studies explicitly assume that vortices do not comprise a critical point.

As long as a core line (or region) does not exclude critical points by definition (streamlines do that explicitly, as stated in section 2.2), a vortex can potentially comprise a critical point at an arbitrary position.

The relation of vortices, critical points and the consequent streamline

patterns are revisited in section 2.4 and 3.2.

Generalized Definitions As mentioned above, core line definitions are computationally more intense. While core regions are based on an isosurface computed from grid points or grid cells, core lines involve various interpolations of values and their reasonable connection. Beside the named definitions based on streamlines from critical points, most definitions are procedural algorithms and therefore implicit. For the same reason, a systematic overview of definitions is complicated.

The *Parallel Vectors Operator* [28] is a “fundamental building block for defining and computing a number of line-type features of vector and scalar fields” [33]. As suggested by Peikert and Roth [28], the thesis at hand employs the operator “as a basis for comparing feature definitions and for reuse of algorithms and implementations”.

2.4 Embedded Vortices

Before presenting vortex core line definitions with the aid of the *Parallel Vectors Operator*, a special type of vortex, an *embedded vortex* as mentioned by Byrne and Cebal [5], is introduced. Without having detailed information about core lines yet, the basic concept of an embedded vortex can be understood by means of the already mentioned idea of a center line and critical points.

According to [5], these structures can be “described by a vortex which is enclosed within a larger vortex flowing in the opposite direction”. The authors refer to concepts of dynamical systems theory, which relate the formation and collapse of embedded vortices over the cardiac cycle to saddle-node bifurcations of equilibrium points [26]. In an unsteady case of vector fields, a saddle-node bifurcation is determined by a pair of critical points, that can be classified as spiral saddle and spiral node (see Figure 2.1), restricted to a common sense of rotation. The inner vortex spirals from the repelling to the attracting critical point, changes orientation and subsequently moves with the outer vortex in the opposite direction. A visualisation of an embedded vortex as well as the illustration of the described behaviour is depicted in Figure 2.4. During the cardiac cycle, the critical points “converge along the core line, collide, and disappear causing a collapse of the embedding and a regression to uni-directional

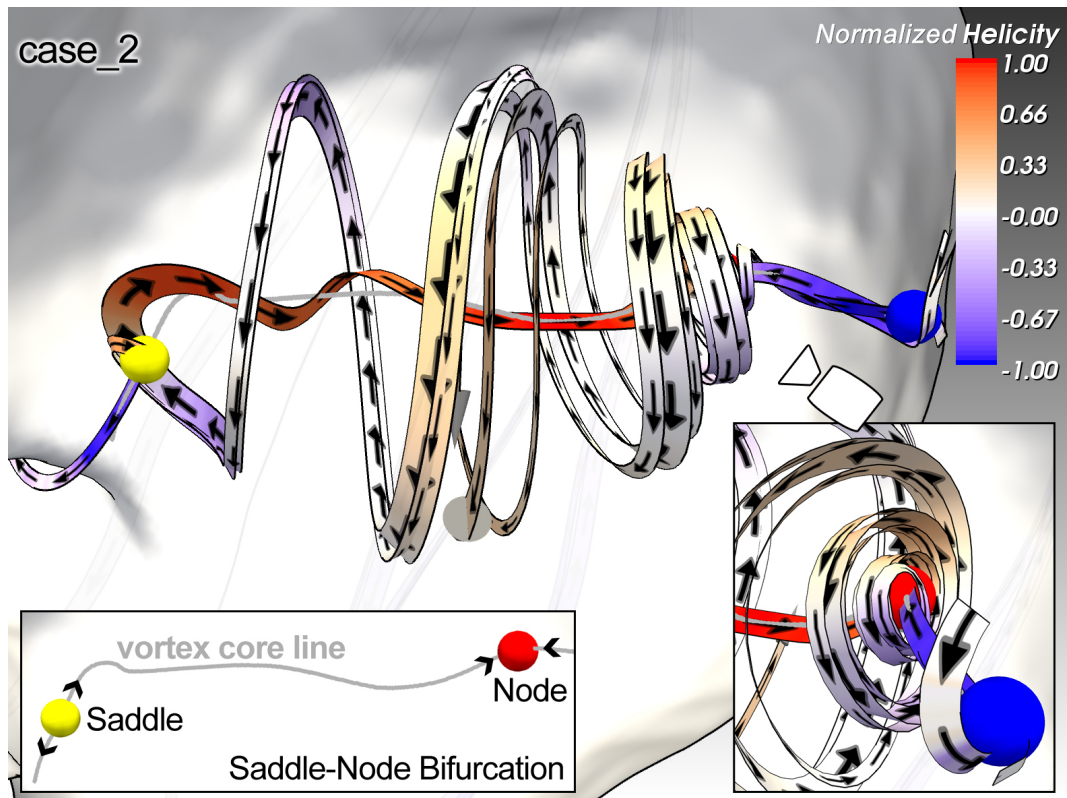


Figure 2.4: Visualisation of an embedded vortex and its characteristic flow behaviour.
© Steffen Oeltze-Jafra

vortical flow” [26].

Although the thesis at hand approaches only steady vector fields, it is possible for a core line to capture an embedded vortex at a time step while the pair of critical points is in the converging state. This fact is revisited in section 3.2.

Chapter 3

Methods

Vortex core lines are extracted by means of the *Parallel Vectors Operator*. The extraction process can be understood as being parameter-free, since thresholds are intended to be chosen without loss of generality. The penalty for this generality is a set of lines that will still contain false positives.

Therefore, further post-processing steps that aim at discarding all false solutions are applied. These steps depends on parameters that have to be set individually with respect to different datasets as well as different core line definitions.

3.1 Parallel Vectors Operator

The *Parallel Vectors Operator* was first published in [28] and is explained in more detail in [33]. For features, such as vortices, there is a lack of explicit definitions. If these were available, it would be easy to distinguish between different feature algorithms based on the mathematical definitions [28]. The operator provides this explicitness by reducing line features to locations where two given vector fields, \mathbf{f} and \mathbf{g} , are parallel. The locations are preliminary to the final result. To map the original feature algorithms exactly, varying additional selection criteria have to be applied. Taking up vortex core *region* definitions, some of these criteria already occurred in the same or a similar manner in section 2.3.2. These selection criteria are binary, thus they label a location as a valid or invalid point. Only the subset of valid points is then used for the following construction of polylines.

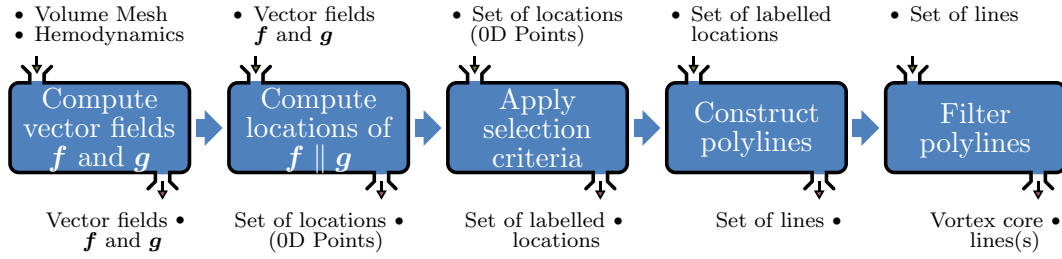


Figure 3.1: Structure of the *Parallel Vectors Operator* accompanying this thesis

Although the operator is based on essential steps, for some of them Roth [33] proposed different variations. In the course of this thesis, a choice concerning these variations is made to the effect that the whole extraction process is free of any parameters. However, the final criterion turned out not to be suitable in the context of aneurysmal blood flow, which is why a new quantity is proposed in section 3.2.

In conclusion and in preview of the next sections, the implementation of the operator accompanying this thesis is based on the structure illustrated in Figure 3.1.

3.1.1 Categories of Line Features

Since the operator is not designed to extract vortex core lines in particular, but line features of vector and scalar fields in general, it provides a categorisation of line features that does not distinctly mark core lines. Instead, different definitions of core lines are assigned to different categories of line features.

Locations of Zero Curvature

The curvature of a streamline is zero at locations where velocity \boldsymbol{v} is parallel to $(\nabla\boldsymbol{v})\boldsymbol{v}$.

$$\boldsymbol{v} \parallel (\nabla\boldsymbol{v})\boldsymbol{v}. \quad (3.1)$$

For steady vector fields, the latter is known as acceleration, the first derivative of \boldsymbol{v} . If these vector fields are parallel, the motion of a fluid particle will momentarily follow the direction of \boldsymbol{v} in a straight line [33].

Sectional Extrema

These extrema are based on the parallelism of a vector field \mathbf{f} and the gradient of a scalar field s .

$$\mathbf{f} \parallel \nabla s \quad (3.2)$$

At these preliminary locations, a vector of \mathbf{f} defines a plane perpendicular to it, in which s has to be an extremum. The kinds of extrema can be evaluated by the scalar's Hessian matrix, projected onto that plane. The additional constraint serves as a selection criterion for this category.

Extremum Lines

Similar to the last category, extremum lines involve extrema in a plane perpendicular to a vector of \mathbf{f} . In contrast, the scalar is replaced by the magnitude of \mathbf{f} .

$$\mathbf{f} \parallel \nabla(\|\mathbf{f}\|) \quad (3.3)$$

In terms of vector parallelism this is equivalent to

$$\mathbf{f} \parallel (\nabla \mathbf{f})^T \mathbf{f}. \quad (3.4)$$

Ridge and Valley Lines

The definition for ridge and valley lines is related to extremum lines and the locations of zero curvature but only considers a single scalar field s . Given that s is a scalar potential, a vector field \mathbf{f} can be written as $\mathbf{f} = \nabla s$. The parallel vectors expression can then be formulated as equation (3.4). Ridge and valley lines are in fact minimum lines of the gradient $\mathbf{f} = \nabla s$ [33]. Because $\nabla \mathbf{f}$ is the symmetric Hessian, the transposition can be omitted, which leads to an equation that looks identical to the condition for zero curvature (3.1).

$$\mathbf{f} \parallel (\nabla \mathbf{f}) \mathbf{f} \quad (3.5)$$

In conclusion, ridge and valley lines are zero curvature lines of the gradient of a scalar potential. To differentiate between ridges and valleys, the Hessian $\nabla \mathbf{f} = \nabla(\nabla s)$ is examined. An example of ridge lines can be seen in Figure 3.2.

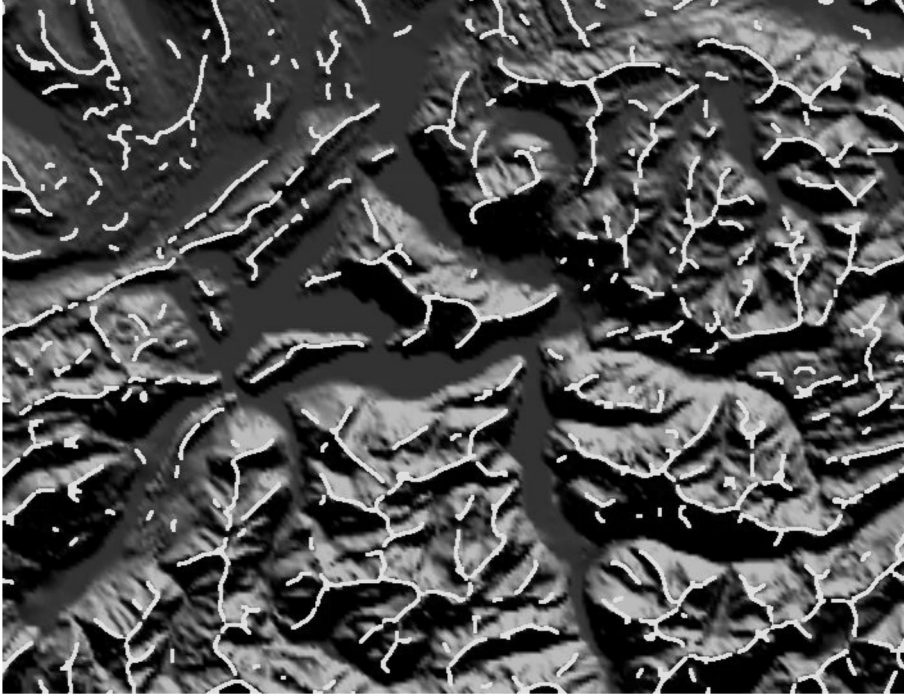


Figure 3.2: Ridge lines of a height field by extracting the zero curvature lines of ∇s and applying the criterion for ridges (two *negative* eigenvalues of the Hessian). Image taken from [33].

General Vector Parallelism

If none of the previous categories apply, the authors speak of a general vector parallelism, which is exactly what the name suggests.

$$\mathbf{f} \parallel \mathbf{g} \tag{3.6}$$

3.1.2 Compute Vector Fields

Every definition is based on two vector fields whose computation is the very first step. Moreover, the choice of these vector fields is what explicitly defines the extraction process. The selection criterion that will be named along with its definition only limits the result to a subset of locations. An overview of the definitions that are compared in the course of this thesis is given in Table 3.1.

Levy, Degani and Seginer

Levy et al. [24] propose to define vortex core lines based on large absolute values of normalized helicity h_n .

$$h_n = \frac{\mathbf{v}}{\|\mathbf{v}\|} \cdot \frac{\boldsymbol{\omega}}{\|\boldsymbol{\omega}\|} \quad (3.7)$$

It is equal to the cosine of the angle between velocity \mathbf{v} and its curl $\boldsymbol{\omega} = \nabla \times \mathbf{v}$. The latter is also known as vorticity. It can easily be translated into a *general vector parallelism*.

$$\mathbf{v} \parallel \boldsymbol{\omega} \quad (3.8)$$

By that, the definition really captures only values of h_n of ± 1 . In the original publication, a selection criterion is *not* proposed. Following the example of Byrne et al. [6], a valid location must exhibit a complex pair of eigenvalues of $\nabla \mathbf{v}$ as well.

Sujudi and Haines

Sujudi and Haines [42] published a core line definition which requires spiralling flow identified by complex eigenvalues of the Jacobian. In particular, they use the real eigenvector to compute a line segment respectively a pair of points. Roth and Peikert [34] show that the latter can be reformulated as velocity \mathbf{v} being parallel to the acceleration.

$$\mathbf{v} \parallel (\nabla \mathbf{v})\mathbf{v} \quad (3.9)$$

In other words, these are *locations of zero curvature*. Still, a complex pair of eigenvalues is a necessary condition for a valid location.

Banks and Singer

The definition of Banks and Singer [1] is a predictor-corrector algorithm. Starting from a seed point, a step in the direction of vorticity $\boldsymbol{\omega}$ is predicted. After that, the step is corrected to the minimum of pressure p in a plane, perpendicular to $\boldsymbol{\omega}$ at the predicted position. The basic idea of the algorithm is depicted in Figure 3.3. Imagining very small step sizes, the procedure finds locations,

where vorticity is approximately parallel to the pressure gradient [33].

$$\boldsymbol{\omega} \parallel \nabla p \quad (3.10)$$

With the additional constraint of pressure minima, this algorithm locates *sectional extrema*. Minima are identified by the projected Hessian having two *positive* eigenvalues. Locations that also satisfy the additional constraint are valid.

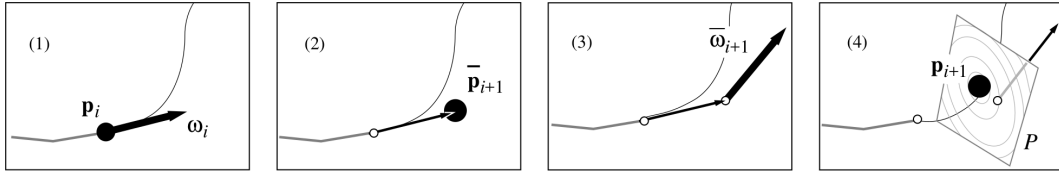


Figure 3.3: Schematic of the predictor-corrector algorithm of Banks and Singer. Image adapted from [1].

Strawn, Kenwright and Ahmad

Strawn et al. [41] use a definition that solely measures vorticity $\boldsymbol{\omega}$ and its magnitude. They look for maxima of the magnitude in planes perpendicular to the vector. This is equivalent to a definition of *extremum lines* of $\boldsymbol{\omega}$.

$$\boldsymbol{\omega} \parallel (\nabla \boldsymbol{\omega})^T \boldsymbol{\omega}. \quad (3.11)$$

Maxima, respectively valid locations, are found when the projected Hessian has two *negative* eigenvalues.

Kida and Miura

In their study, Kida and Miura [22] defined a pressure-like value, derived from the divergence of acceleration. As an approximation, the authors always use the real pressure p and identify a vortex core line by connected locations of pressure minima. These locations can be reinterpreted as *ridge and valley lines* of pressure.

$$\nabla p \parallel (\nabla(\nabla p)) \nabla p \quad (3.12)$$

The Hessian, $\nabla(\nabla p)$, has two *positive* eigenvalues for a valley. This again identifies a valid location.

Roth and Peikert

Roth and Peikert [34] carry on the idea of *locations of zero curvature* by including higher order derivatives. All previous studies implicitly assumed piecewise linear flows, by only including first derivatives in the calculations. According to the authors, this only models core lines that are straight lines. Especially if the whole flow is curved, a core line could also be bent [33] (see Figure 3.4). In a steady vector field, acceleration $\mathbf{a} = (\nabla \mathbf{v})\mathbf{v}$ is derived from velocity \mathbf{v} . A general vector parallelism that includes the second derivative of \mathbf{v} can then be expressed as

$$\mathbf{v} \parallel (\nabla \mathbf{a})\mathbf{v} \quad (3.13)$$

or

$$\mathbf{v} \parallel \nabla((\nabla \mathbf{v})\mathbf{v}). \quad (3.14)$$

To stress that this definition is a higher-order variant of [42], it could be named *locations of zero torsion* [33]. Independent of higher order derivatives, a valid location is restricted in almost the same manner as in [42]: Before $\nabla \mathbf{v}$ is checked for a complex pair of eigenvalues, it is projected onto the plane perpendicular to the core velocity.

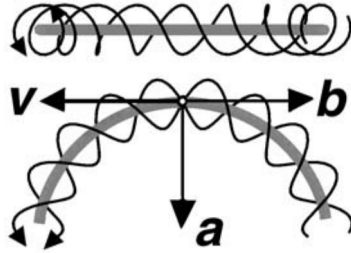


Figure 3.4: Front and top view of a bent core line with $\mathbf{b} = (\nabla \mathbf{a})\mathbf{v}$. Image taken from [34].

3.1.3 Compute Locations

The fundamental idea of the operator is to find locations of parallel vectors on the faces of each grid cell. This results in a set of locations of which every

Authors	Year	Keywords
Levy, Degani and Seginer	1990	<i>normalized helicity</i>
Banks and Singer	1995	<i>sectional minima of pressure</i>
Sujudi and Haines	1995	<i>lines of zero curvature</i>
Kida and Miura	1997	<i>valley lines of pressure</i>
Strawn, Kenwright and Ahmad	1998	<i>extremum lines of vorticity</i>
Roth and Peikert	1998	<i>higher-order derivatives</i>

Table 3.1: Overview of vortex core line definitions compared in this thesis

location corresponds to a unique face. In fact, the locations are based on analytic solutions calculated on triangles. Therefore, if necessary, the faces of each grid cell are split into 2-simplices. Special care has to be taken of face duplicates of adjacent cells and their identical splitting. The set of locations and especially the relation between a location and its corresponding triangle serves as a basis for subsequent steps. Because it is only about the parallelism of two given vector fields, the following analytic method is common to all definitions.

On a triangle ABC , linear interpolants $\hat{\mathbf{f}}$ and $\hat{\mathbf{g}}$ for the two vector fields \mathbf{f} and \mathbf{g} can be written as

$$\hat{\mathbf{f}} = \mathbf{F} \begin{pmatrix} s \cdot h \\ t \cdot h \\ h \end{pmatrix} \quad \text{with} \quad \mathbf{F} = \begin{pmatrix} \mathbf{f}_A - \mathbf{f}_C & \mathbf{f}_B - \mathbf{f}_C & \mathbf{f}_C \end{pmatrix} \quad (3.15)$$

and

$$\hat{\mathbf{g}} = \mathbf{G} \begin{pmatrix} s \cdot h \\ t \cdot h \\ h \end{pmatrix} \quad \text{with} \quad \mathbf{G} = \begin{pmatrix} \mathbf{g}_A - \mathbf{g}_C & \mathbf{g}_B - \mathbf{g}_C & \mathbf{g}_C \end{pmatrix}. \quad (3.16)$$

The variables s , t and a constant 1 can be interpreted as affine homogenous coordinates for the given triangle. Two vector fields are parallel when

$$\mathbf{F} \begin{pmatrix} s \\ t \\ 1 \end{pmatrix} = \lambda \mathbf{G} \begin{pmatrix} s \\ t \\ 1 \end{pmatrix}. \quad (3.17)$$

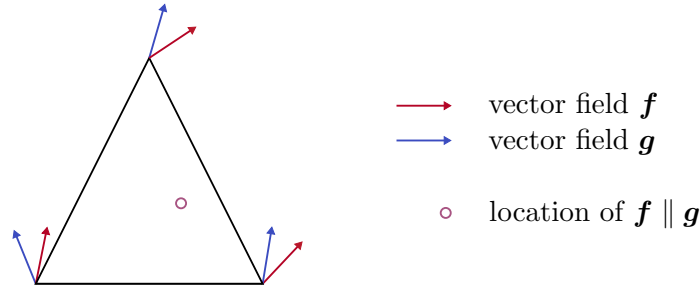


Figure 3.5: Two vector fields being parallel at a highlighted location on a triangle.

A rearrangement of the equation leads to an eigenvector problem.

$$\mathbf{G}^{-1}\mathbf{F} \begin{pmatrix} s \\ t \\ 1 \end{pmatrix} = \lambda \begin{pmatrix} s \\ t \\ 1 \end{pmatrix} \quad (3.18)$$

If \mathbf{G} is singular and \mathbf{F} is not, the roles can be swapped. Otherwise no solution exists.

The outcome of equation (3.18) are eigenvectors that are intended to describe points in the local coordinate system of the given triangle, which is the *real* plane. However, these eigenvectors may be complex referring to points within the *complex* plane. In these cases, no geometric interpretation for the current purpose exists, which is why these eigenvectors are omitted.

Given that equation (3.18) yields a real eigenvector, an additional constraint for the resulting point is to lie inside of the triangle. Furthermore, only the first solution is stored for each triangle which is necessary for the topology-based construction of polylines in section 3.1.5.

Figure 3.5 illustrates a point inside of a triangle, which is a location where the vector fields \mathbf{f} and \mathbf{g} are parallel.

3.1.4 Apply Selection Criteria

For every location, an additional selection criterion is applied that labels the point as valid or invalid. The reformulated definitions in section 3.1.2 involve selection criteria that measure the velocity gradient or the Hessian of a scalar. The necessary values are available on the grid nodes or can be derived from them, as they are closely related to the vector parallelisms (see section 3.1.2). Every

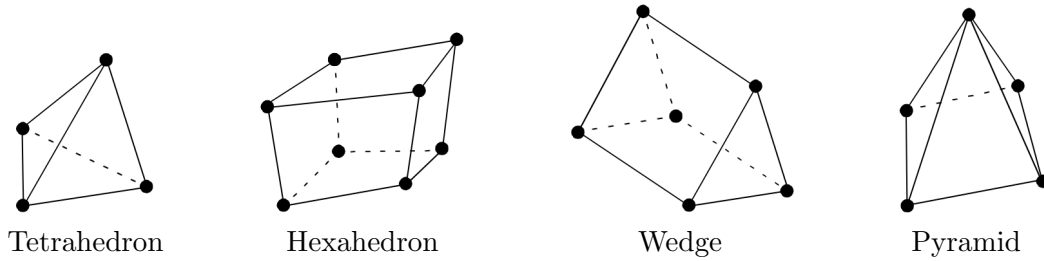


Figure 3.6: Different cell forms that might occur in an unstructured grid. Illustration adapted from [40].

location refers to the three grid nodes, that were involved in its computation based on triangle (see Figure 3.5). For a location to be labelled valid the selection criterion has to turn out valid at all three nodes.

3.1.5 Construct Polylines

Up to this point, the extraction process led to a set of unconnected points. These points are found on triangles that belong to two adjacent cells or a single cell. The latter occurs if the face is on the boundary of the domain.

From a cell's point of view, a triangular face can be one of the initial triangles, that are induced by the cell form, or a triangle that originated from the splitting of a non-triangular face. Different cell forms are illustrated in Figure 3.6. Connections 'through' a cell (line segments) are constructed based on two rules.

1. If a valid point is found on both triangles of a splitted face, only the 'first'¹ one is considered while the other one is omitted. This choice is a reasonable simplification, since it only slightly changes the path of a line segment but not the affiliation to the original non-triangular face.
2. If the overall number of considered valid points is two, these points are connected by a line segment. This case is illustrated in Figure 3.7.

In every other case, the whole cell is disregarded and no line segment is constructed. A cell with more than two valid points on its faces is assumed to

¹*first* refers to the point, that was first stored during the computations in section 3.1.3 and is determined by the underlying implementation of the 'Parallel Vectors Operator'.

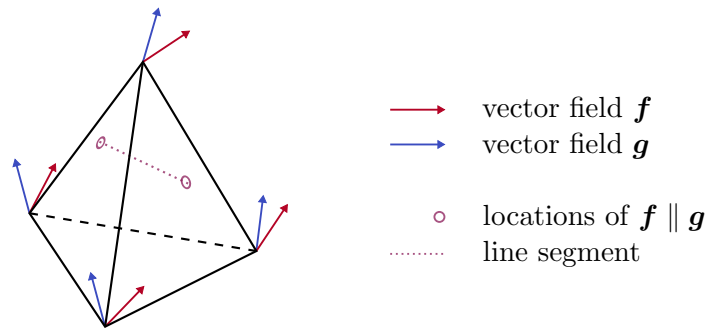


Figure 3.7: A line segment is constructed from two locations that lay on a cell's surface.

be an invalid cell, since a vector parallelism on three or more sides of a cell is not sensible in the context of spatial flow data.

Because almost every point belongs to a face that is shared by two cells, line segments that contain a mutual point can be concatenated. This way, the grid topology is used to construct polylines from line segments.

3.1.6 Filter Polylines

As described above, polylines are constructed from valid points regardless of the polyline's length or the number of comprised points. However, a polyline has to be composed of at least three points. This minimum is accounted for by the computation of core line tangents in the next steps.

Until now, the implementation of the operator followed the suggestions of [28] and [33] and leaves a set of polylines. As a next step, the authors propose to apply yet another criterion that measures an angle in order to eliminate false positive parts. At this stage, the implementation of the operator accompanying this thesis deviates from the original publication by proposing and using a more suitable criterion for the context of aneurysmal blood flow, which is discussed in the next section.

3.2 Angle Criteria

Depending on the pair of vectors, involved in varying angle criteria, different characteristics arise that are examined with respect to vortices and critical points respectively embedded vortices.

Core Line Tangent — Velocity

In the original publications covering the *Parallel Vectors Operator* [28, 33], the authors define the *feature strength*, that measures the cosine of the angle between core line tangent \mathbf{t} and core line velocity \mathbf{v} at a given point.

$$|\cos \alpha| = \left| \frac{\mathbf{v}}{\|\mathbf{v}\|} \cdot \frac{\mathbf{t}}{\|\mathbf{t}\|} \right| \quad (3.19)$$

By taking the absolute value, it only gives information about the angle, not about the orientation of vectors. To disregard the orientation is reasonable because the tangent's orientation depends on the arbitrary situation whether the core line is sampled from the one or the other end. The described angle is expected to be low along true positive parts, because the rotary motion of a vortex does not occur in a plane, but is stretched along the whole core line reducing the angle.

These lines are connections of points, which are based on vector parallelism. However, the parallelism at a single point is independent of the core line, of which it is part. As a consequence, there is no indication that the core line always follows the trajectory of a streamline through the velocity field. Hence, in [33], the angle between core line tangent and core line velocity is restricted to be smaller than 45° (30° in a stricter manner) without exception. In due consideration of critical points that can occur along a core line and embedded vortices in particular, this procedure is disadvantageous. In the segment around the attracting critical point, the flow of the inner vortex changes direction and moves with the outer vortex. For a core line that has captured an embedded vortex the angle between its tangent and the local velocity would reach a maximum in that segment. For the repelling critical point, and for other possible spiral saddles or spiral nodes, that do not emerge in linkage of an embedded vortex on the core line, the angle reaches a maximum as well, due to the attracting or repelling characteristic. As a consequence, strict filtering based on the angle criterion would systematically cut out segments around critical points.

Velocity — Vorticity

Although originally intended to be a core line definition [24], normalized helicity can also serve as an universal angle criterion that discards false positives. It is defined as the cosine of the angle between velocity \mathbf{v} and vorticity $\boldsymbol{\omega}$ and measures “the degree of knottedness of tangled vortex lines” [24]. In [6], core lines were restricted to be composed of line segments that exhibit extremums of normalized helicity over a tetrahedral element.

This quantity has similar characteristics to the aforementioned. The more stretched a vortex is along its core line, the lower the angle between velocity and vorticity. Particular attention has to be paid once more to critical points and embedded vortices. Since normalized helicity is the cosine of an angle, a change of sign indicates a change of orientation of \mathbf{v} or $\boldsymbol{\omega}$. Oeltze et al. [26] state that for embedded vortices “the direction of $\boldsymbol{\omega}$ is stable along the core line”. Whereas in section 2.4, the direction of \mathbf{v} was described as unstable, due to a change of the direction of flow in the segment around the attracting critical point. For core lines that represent embedded vortices the sign of normalized helicity flips in these segments while the values approach zero. In other words, the angle between velocity and vorticity reaches a maximum, similar to the angle mentioned before. The same applies again for single critical points of type spiral saddle or spiral node. A strict filtering based on extrema of normalized helicity would cut out segments around critical points as well.

Nevertheless, if the purpose is to specifically locate critical points of a spiralling type along the core line, as done among other things in [26], a changing sign of normalized helicity serves as a perfect indicator provided that the local flow exhibits a rotary motion.

Core Line Tangent — Vorticity

In the preceding paragraphs, true positive parts of core lines were almost everywhere characterised by small angles of both discussed quantities. Embedded vortices, as well as single spiralling saddles and spiralling nodes as an exception, feature maximal angles in short segments of the core line. Especially in the context of cerebral aneurysms, it would be useful to find a quantity that features consistent values along true positive parts, independent of critical points and thus the kind of vortex it has captured.

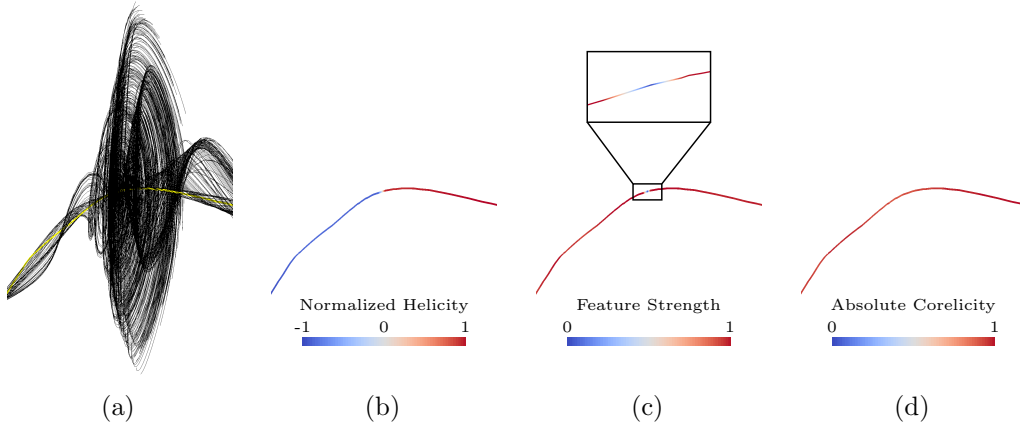


Figure 3.8: A vortex core line containing a critical point. (a) Streamlines are seeded along the core line. Values of (a) normalized helicity, (b) feature strength and (c) absolute corelicity are plotted.

To achieve the very same thing, the essential characteristics of both herein before mentioned criteria are combined in a new quantity, *normalized corelicity* c_n , defined as

$$c_n = \frac{\mathbf{t}}{\|\mathbf{t}\|} \cdot \frac{\boldsymbol{\omega}}{\|\boldsymbol{\omega}\|}. \quad (3.20)$$

Since the orientation of vorticity $\boldsymbol{\omega}$ was described as stable for the problematic case of embedded vortices (implicitly involving the case of a single critical point), the sign only depends on the direction in which the core line is sampled. In order to be independent of that direction, the *absolute corelicity* is defined by taking the absolute value of normalized corelicity. In other words, this quantity measures the cosine of the angle between core line tangent \mathbf{t} and core line vorticity $\boldsymbol{\omega}$.

$$|\cos \gamma| = |c_n| \quad (3.21)$$

Because the angle γ is a more intuitive quantity, it is used in the next sections and is referred to as the *corelicity angle*. In terms of using one of the new quantities as a parameter, it is just a matter of agreement whether the absolute corelicity, ranging from zero to one, or the corelicity angle, ranging from 0° to 90° , is used. Figure 3.8 illustrates the consistent distribution of high absolute corelicity (respectively a low angle) along the core line particularly covering the segment that comprises a critical point. Whereas, no general statement can be made about false positive parts.

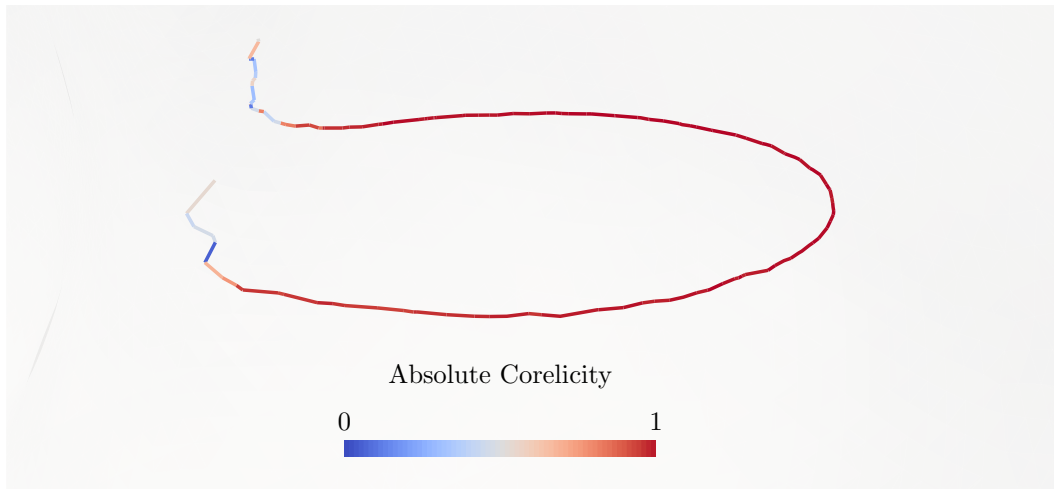


Figure 3.9: False positive ends of an actual true positive core line

3.2.1 New Criterion

In order to replace the angle criterion of the original publication with the measurement of the corelicity angle, a combination of two steps is proposed.

First Step The first step is similar to the filtering in section 3.1.6 but is based on a rough threshold on corelicity angle (60°) combined with a moderate tolerance of successive angle violations. It is intended to discard parts that are false positives in a general comprehension. The need of this step is most evident for polylines that mainly consist of a true positive part but also include false positive ends as illustrated in Figure 3.9. With these parts of high corelicity angles being excluded from the set of polylines, a subsequent step that assesses an average value per line can further differentiate true and false positives.

Second Step Since only a rough threshold was applied to the polylines, true positives still show their uniform distribution of low corelicity angles in contrast to false solutions whose distribution is more diverse. In this second step, decisions are made for entire lines, based on the average values of corelicity angle that are derived from the individual values at every point of the line. Another threshold filters out a subset of polylines that have an average corelicity angle smaller than 45° . Besides false positives, this value is intended to generally comprise all true positives.

3.3 Post-Processing

The post-processing depends on parameters that have to be adjusted individually for every combination of dataset and core line definition. Since the absolute corelicity has convenient properties concerning core lines, especially the distinction between true and false positives, it is used in another step to further exclude false solutions. In combination with a threshold on the minimal length of polylines, false positives can be discarded to the greatest possible extent.

Post-Processing Filtering The filtering occurring in the post-processing can be understood as a stricter and at the same time user-driven version of the *first step* in section 3.2.1. It depends on two parameters, the maximal corelicity angle γ and the maximal number of violations of that angle. To discard as much false positives as possible, these parameters have to be set individually with respect to different datasets and underlying core line definitions. The stricter the parameters, the more fragmented the final result becomes.

Threshold on Length Actually, the above-mentioned parameters also depend on the individual shapes of lines that belong to a single dataset. However, in the majority of practical examples that were examined in the course of this thesis the remaining false positives at this stage were shorter than the shortest true positive. Hence, a length filter can be used to remove *all* false solutions. In the case of a true positive that is shorter than a false solution the implementation is not able to separate both groups flawlessly.

Chapter 4

Comparison

To compare six vortex core line definitions that have been presented in section 3.1.3 the *Parallel Vectors Operator* was applied to seven datasets of ruptured aneurysms, for each definition individually. For one thing, lines were compared *qualitatively* to examine which and to which extent vortices of a dataset are found by different vortex definitions. For another thing, a *quantitative* comparison estimated the amount of false positives.

Throughout the following sections, the different algorithms are abbreviated by their author's initials:

sh: Sujudi, Haimes (lines of zero curvature)

lds: Levy, Degani, Seginer (normalized helicity)

rp: Roth, Peikert (higher-order derivatives)

ska: Strawn, Kenwright, Ahmad (extremum lines of vorticity)

bs: Banks, Singer (sectional minima of pressure)

km: Kida, Miura (valley lines of pressure)

It should be noted that the definitions of **bs** and **km** additionally require pressure information. Since this quantity is directly associated with velocity during a simulation, its availability is only a matter of data export.

4.1 Qualitative Comparison

The qualitative comparison is based on a visual inspection of vortex core lines and their resulting streamline patterns. In particular, it makes use of the output of the *Parallel Vectors Operator* without any post-processing, since the set of lines at this stage does not depend on any user-defined parameters. The penalty for this generality is a set of lines that still contains false positives. However, the *qualitative* comparison only evaluates which and to which extent vortices are found.

Firstly, overall assumptions on the actual number of vortices per dataset and their types were made by means of the lines of *all* compared definitions. The number of vortices was assumed on the basis of stream lines seeded from the pooled set of lines while the type of a vortex was determined by the lines' profiles of normalized helicity. As pointed out in section 3.2, a changing sign of normalized helicity indicates a critical point of a spiralling type. The type of a vortex is referred to as follows:

Embedded Vortex (EV): a vortical structure featuring a saddle-node bifurcation

Critical Point Vortex (CPV): a vortex comprising a single critical point

Well-Defined Vortex (WDV): a vortex without any critical points

Subsequently, the definitions were examined individually, regarding to which extent vortices were found completely (by continuous core lines) or incompletely (by fragmented or too short lines).

Overall Assumptions A streamline structure was counted as a vortex if the streamlines indicated a rotary motion around a common axis. This 'common axis' can be understood as a fuzzy guide, that arises from streamline patterns of multiple shifted lines or an individual one. Subsequently, the type of the vortex was determined. Therefore, the profiles of normalized helicity of core lines, from which the corresponding streamlines had been integrated, were examined. If a changing sign of normalized helicity was found in each two distinct segments on involved core lines in combination with the characteristic stream line pattern described in section 2.4, an EV was assumed.

<i>dataset</i>	<i>an_01</i>	<i>an_10</i>	<i>Case_347</i>	<i>Case_380</i>	<i>Case_381</i>	<i>Chlg_1</i>	<i>Chlg_2</i>
sh	⊙⊗	⊙⊙⊙⊙⊙	⊙	⊙⊙⊗⊗	⊗	⊗	⊙⊙
lds	⊙⊗	⊙⊙⊙⊙⊙	⊙	⊙⊙⊗⊗	⊗	⊗	⊙⊙
rp	⊙⊗	⊙⊙⊙⊙⊙	⊙	⊙⊙⊗⊗	⊗	⊗	⊙⊙
ska	⊙⊗	⊙⊙⊙⊙⊙	⊙	⊙⊙⊗⊗	⊗	⊗	⊙⊙
bs	⊙⊗	⊙⊙⊙⊙⊙	—	—	—	—	—
km	⊙⊗	⊙⊙⊙⊙⊙	—	—	—	—	—

Table 4.1: (⊙) Well-Defined Vortex, (⊙) Critical Point Vortex, (⊗) Embedded Vortex, (■) Vortex not found, (■) Vortex partly found, (■) Vortex entirely found,

The same procedure applied for CPVs, but for a single change of sign. However, if the sign did not change, the vortex was assumed to be well-defined. To differentiate WDV from turbulent flow, a common axis was essential.

Individual Examinations A line, running with the common axis of a structure that had been assumed to be a vortex in the last paragraph, labelled the vortex as *found*. If this line did not capture the whole rotary motion around the axis or if more than one core line did, the vortex was labelled as ‘partly found’. Otherwise, it was ‘entirely found’ by a single core line. Lastly, if a vortex was not captured by any line, it was labelled as ‘not found’.

An overview of the results for the qualitative comparison is given in Table 4.1. Based on the visual inspection, the number of icons in Figure 4.1 represent the assumed total number of vortices per dataset.

Qualitative Score Based on the results of Table 4.1, the vortex core line definitions are scored on the basis of points. The resulting score is the quotient (in percent) of a definitions’s total number of points divided by the maximal

Definition	Qualitative Score
sh	90%
lds	96%
rp	72%
ska	19%
bs	50%
km	29%

Table 4.2: Qualitative score of vortex core line definitions

number of points it could have reached (see Table 4.2). For the total number of points, the vortices of all datasets are awarded: A vortex entirely found gets two points, a vortex partly found gets one point and a vortex that was not found at all gets zero points. The maximal number is the sum of points if all vortices were found to their full extent.

4.2 Quantitative Comparison

Besides the visual inspection of a dataset, a quantitative estimation of the relation between true and false positives is of common interest. It indicates the precision of a definition, which is in turn a measure of the definition's quality or exactness. To quantify the necessary values of true and false solutions, post-processing steps, as proposed in section 3.3, were carried out. As already mentioned in the corresponding section, these steps depend on parameters that need to be adjusted for every combination of dataset and vortex definition individually.

On the one hand, the post-processing cannot ensure, that all false positives can be discarded, while on the other hand, a strict setting of parameters can exclude true positives from the final set of lines. In terms of comparing the exactness of definitions, both cases are undesired. However, in the course of this thesis, a set of parameters that perfectly separates true from false solutions could not be found for every dataset and definition. Nevertheless, an overview of optimal parameters, in terms of not excluding any core line that belongs to a vortex that had been found by the visual inspection, is given in Table 4.3.

Fraction of False Positives Directly associated with the sets of parameters are the fractions of false positives that can be taken from Table 4.4. The values are measured by means of the lengths of line segments, of which core lines (polylines) are composed.

Given the i^{th} polyline that is composed of n points its length L_i is the sum of the individual euclidean distances between two successive points.

$$L_i = \sum_{k=1}^{n-1} \|p_k - p_{k-1}\| \quad (4.1)$$

<i>dataset</i>	<i>an_01</i>	<i>an_10</i>	<i>Case_347</i>	<i>Case_380</i>	<i>Case_381</i>	<i>Chlg_1</i>	<i>Chlg_2</i>
sh	30/1/1	35/4/0.3	20/30/1	25/3/0.6	35/10/0.5	30/4/1	30/7/3.5
lds	27/1/1.5	45/1/0.4	20/30/1	25/3/0.6	35/20/0.5	50/1/3	30/4/4
rp	30/1/0.5	40/2/0.4	20/30/1	25/7/0.3	40/20/0.2	30/4/1	30/3/3
ska	—	35/1/1.5	—	—	—	—	20/2/2.5
bs	30/1/0.5	35/5/2	—	—	—	—	—
km	35/2/0.4	40/1/1.1	—	—	—	—	—

Table 4.3: Optimal parameters for post-processing:
maximal γ / maximal violations of γ / minimal core line length

<i>dataset</i>	<i>an_01</i>	<i>an_10</i>	<i>Case_347</i>	<i>Case_380</i>	<i>Case_381</i>	<i>Chlg_1</i>	<i>Chlg_2</i>
sh	0.358*	0.118*	0.394	0.483	0.689	0.211	0.560
lds	0.780*	0.198*	0.284	0.549	0.589	0.637	0.665
rp	0.633*	0.316*	0.770	0.691	0.634*	0.760	0.839
ska	1	0.737*	1	1	1	1	0.922
bs	0.310*	0.203	—	—	—	—	—
km	0.543*	0.745*	—	—	—	—	—

Table 4.4: Estimated fraction of false positives
(*) The post-processing was not able to discard all false positives

The summed up length of all unprocessed lines (direct output of the operator) is denoted as L_{pv} , while for the set of lines *after* post-processing their sum is denoted as L_{pp} . Based on these values, the fraction of *true* positives can be estimated as

$$r_t = \frac{L_{pp}}{L_{pv}}. \quad (4.2)$$

Therefrom results the fraction of false positives r_f among the output of the *Parallel Vectors Operator* as

$$r_f = 1 - r_t. \quad (4.3)$$

It has to be noted that for cases marked with an asterix (*), the post-processing was not able to discard all false positives. On the one hand, this led to an increased value of r_t respectively a decreased value of r_f . On the other hand, the definitions to which this applied showed a higher absolute value of false positives generally which is why the distorted values are assumed to be comparable nevertheless.

4.3 Results

In the following, the various *true positive* results, as they were included in the qualitative comparison, are described for every dataset individually. Hence, the accompanying figures rest upon the parameters described in the quantitative part of the comparison. The visualisations show the vortex core lines of all definitions separated by distinct colours, that can be gathered from the captions. Critical points are slightly indicated by black circles. Since the purpose of the comparison is to show differences in the core line's paths, no smoothing is applied.

an_01: (Figure 4.1) The core lines of **sh**, **lds** and **rp** capture the two vortices to their full extent and only differ slightly in length. While they meet the center axes of both vortices, the core lines of **bs** and **km** strongly depart from the others in the bent section. The spacing from the actual axis can also be seen to a lesser extent at the straight axis of the other vortex. By these 'gaps', they miss two critical points besides the one that is not captured by both definitions at all. The definition of **km** produces the shortest and at the same time incomplete lines, while longer lines of **bs** solely find the straight vortex to its full extent.

an_10: (Figure 4.2) The largest structure of a WDV is found by all definitions with the exception of **ska** that lacks the right end of the vortex. The CPV on the right side in Figure 4.2 is captured to a diverse extent. While the definitions of **sh** and **bs** extract an entire core line, the others solely find individual parts which include or not include the critical point. In the foreground of Figure 4.2, two small CPVs are found by the definitions of **sh**, **lds** and **rp**. If the lines capture the critical point, the vortex is considered as entirely found. Another vortex that is not visualised in the accompanying figure is solely found by core lines of **lds** and **ska**.

In this particular dataset, the smaller vortices are captured to different extents, which could be an indication of a rotary motion, that is not as distinct as for the large structure. Their rotation could be primarily caused by critical points as well. Additionally, the

datasets *an_01* and *an_10* exhibit lower grid resolution in contrast to the others.

Case_347: (Figure 4.3) The definitions of **sh**, **lds** and **rp** extract vortex core lines that successfully represent the vortex' full extent. It has to be noted that the definition of **rp** produces a shorter core line, ending at the critical point. The extended lines of the other definitions represent a segment, that not necessarily belongs to the vortex structure. It rather indicates a region in which the vortical motion, caused by the critical point, decreases.

Case_380: (Figure 4.4) At first sight, the definitions of **sh**, **lds** and **rp** produce consistent results and all vortices of the dataset can be visualised by means of the single sets of lines. On closer examination, the definition of **rp** actually exhibit three individual lines separated by two small gaps for the bent EV. In fact, this line features five critical points, of which four form a double EV while the third can be understood as an isolated critical point. In the segment around the latter critical point, the first gap is found. It is a 'real' gap, where no valid locations had been found. Intuitively, one would expect this gaps to be closed, since a short connection of mutually opposite endings is reasonable. The second gap is located near the double EV. Its occurrence can be attributed to the construction of polylines in section 3.7 which disregards cells with more than two valid points. The gap indicates that multiple valid points on a cell's faces *can* contain a 'correct' pair and that the cell as a whole can not be disregarded in general.

Case_381: (Figure 4.5) The results in this case are similar to *Case_380* to the effect, that a gap, caused by a disregarded cell, is responsible for the incomplete detection of the vortex structure. This affects again the definition of **rp** while the others do not show this peculiarity but instead produce almost identical results. It is conspicuous, that the core lines of **rp** are more winding in contrast to the other lines. A similar behaviour can also be noted for *Case_347*.

- Chlg_1:* (Figure 4.6) The dataset features a large EV that is found by the definitions of **sh** and **lds**, while the definition **rp** finds two individual core lines. In contrast to *Case_380*, where one would expect the endings to be connected, these should not, because of the gap's significant width. However, all true positive lines are in close proximity to each other.
- Chlg_2:* (Figure 4.7) The results for this dataset can be divided in two groups. The first group contains the definitions of **sh** and **lds** that successfully detect both vortices to its full extent and comprise almost the same locations. In contrast, the second group of **rp** and **ska** finds individual parts of the vortex located in the vessel. Compared to the other results, the core line of **rp** is too short, whereas the definition of **ska** produces a small gap. This time, the gap can no be traced back to a disregarded cell.

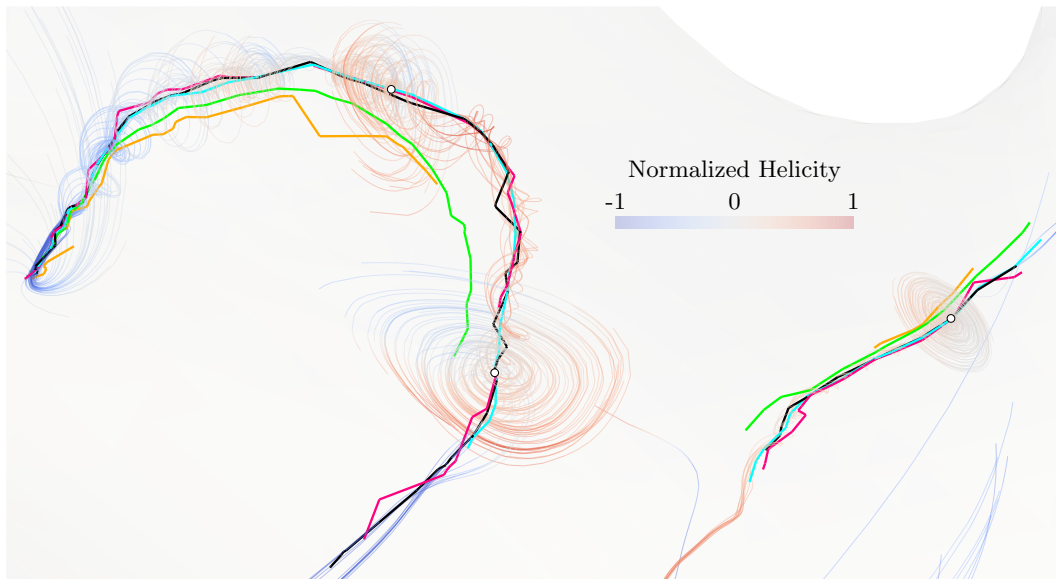


Figure 4.1: Results of dataset *an_01*
(■) sh, (■) lds, (■) rp, (■) bs, (■) km,

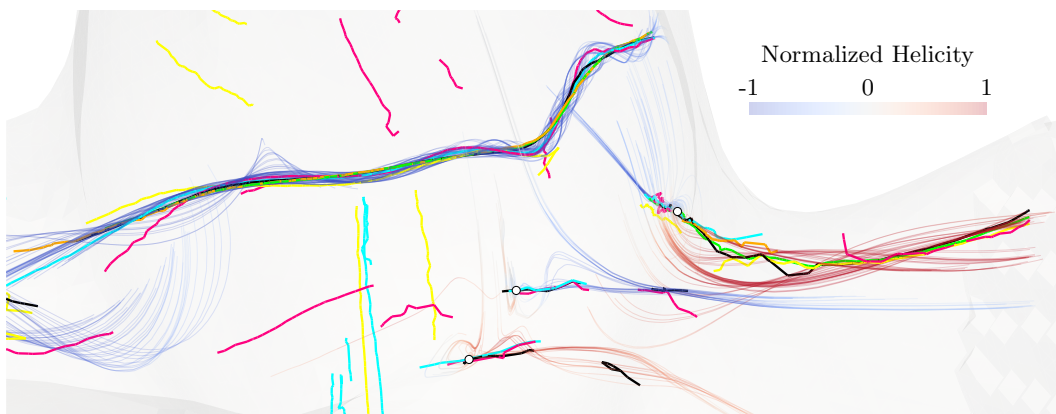


Figure 4.2: Results of dataset *an_10*
(■) sh, (■) lds, (■) rp, (■) ska, (■) bs, (■) km,

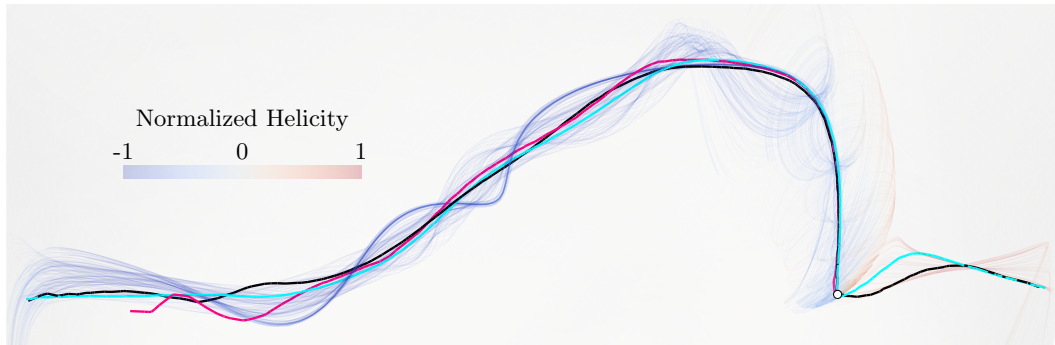
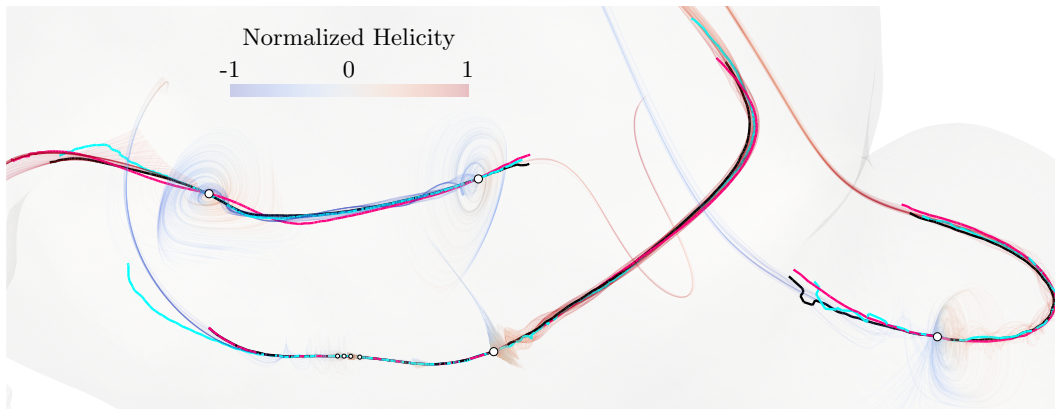
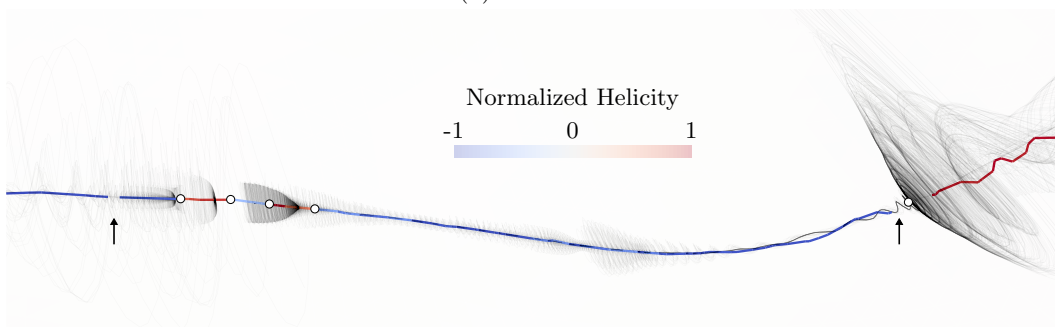


Figure 4.3: Results of dataset *Case_347*
 (■) sh, (■) lds, (■) rp



(a) Overview



(b) Core line, that features two gaps (arrows).

Figure 4.4: Results of dataset *Case_380*
 (■) sh, (■) lds, (■) rp

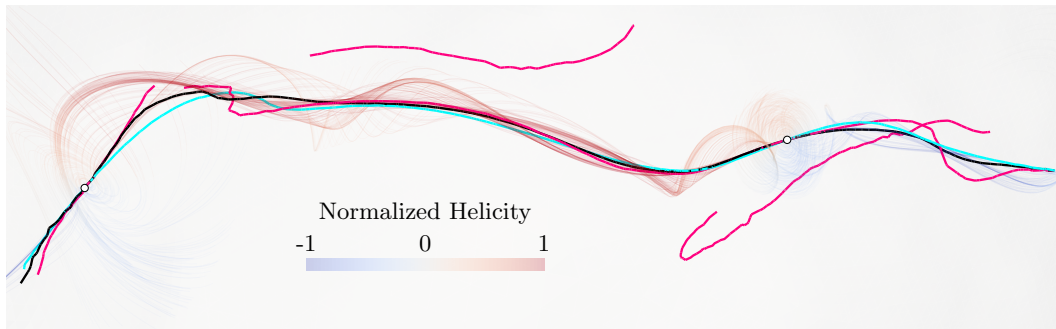


Figure 4.5: Results of dataset *Case_381*
(■) sh, (■) lds, (■) rp

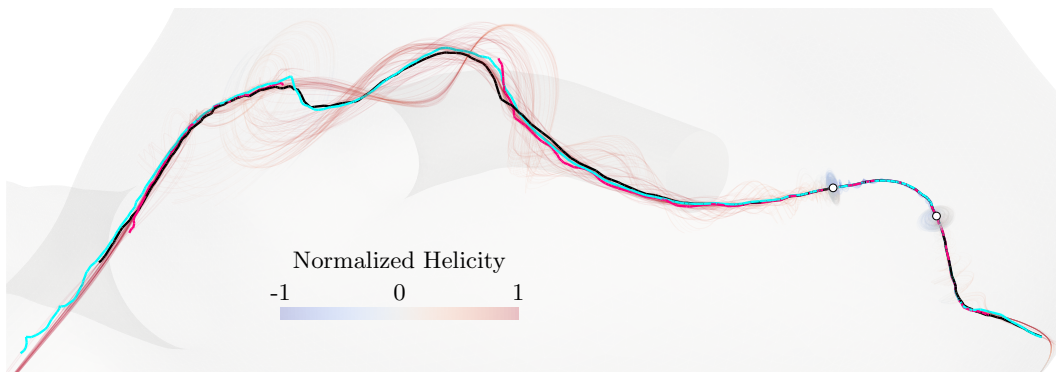


Figure 4.6: Results of dataset *Chlg_1*
(■) sh, (■) lds, (■) rp

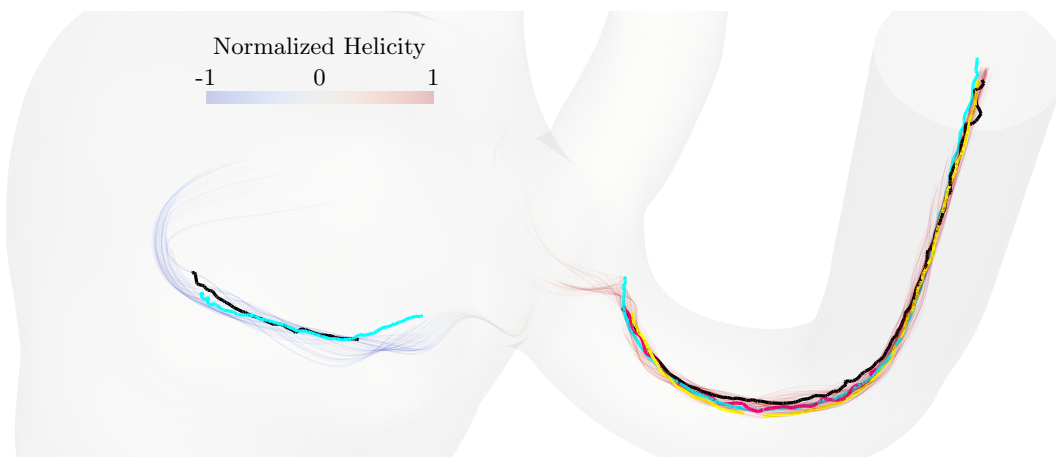


Figure 4.7: Results of dataset *Chlg_2*
(■) sh, (■) lds, (■) rp, (■) ska,

Chapter 5

Discussion

An interpolation between multiple sets of lines from several vortex definitions is not reasonable, due to the significant amount and diverging distribution of false positives at the parameter-free stage. Especially the high variation among definitions for the same dataset complicates any attempt to unify their results.

Although different approaches to unify the lines are conceivable, one would have to know beforehand, which lines are relevant for the current purpose. Relevant lines would probably be true positives or lines close to them, resulting in the necessity of post-processing steps. In fact, one could *interpolate* between the lines after they were processed in datasets like Case_347, resulting in a set of lines that minimizes the error with respect to the original sets. Obviously, this procedure would not be very reasonable, since optimal parameters for a number of datasets would have to be found, if that possible, for all definitions.

As a consequence, it is more efficient to find a best definition, that finds vortices in the majority of cases and to invest an overhead in the lines' post-processing.

Based on the qualitative comparison in section 4.1 and the qualitative scores (see Figure 4.2), the vortex definition of Levy et al. [24] succeeded in most datasets. The only vortex, where an entire detection failed, belongs to a dataset whose grid resolution is significantly lower, compared to the majority of others. Additionally, the mentioned vortex was only partly or not at all found by other definitions indicating that it does exhibit a motion, that is not as intuitive as the others.

The definition of Levy et al. [24] was additionally restricted to complex

eigenvalues of $\nabla\mathbf{v}$. This decision was made, due to the original definition not featuring an additional selection criterion. At the same time, it only discards solutions without altering the characteristic definition of the vector parallelism. The addition of that criterion can be evaluated as successful, since it was possible to discard all remaining false positives by the successive post-processing in the majority of cases.

Since the flexibility of an own implementation is not always given, the definition of Sujudi and Haines [42], that often serves as the recommended standard implementation, can be assessed just as good. Both vortices, that were not found by their definition were rarely found by others indicating that these vortices exhibit a fuzzy rotary motion, in contrast to a strong rotation around a clear axis of a significant length.

The definition of Roth and Peikert exhibit an unique characteristic regarding grid cells with more than two valid points on the cell's faces. In two cases, these disregarded cells gave rise to gaps, that cut a true positive line in multiple pieces. As a consequence, the corresponding vortices were labelled only as partly found, according to the qualitative comparison. Another characteristic is the more winding shape of true positives which could be explained by the inclusion of higher order derivatives in the definition. In comparison to both already mentioned definitions, the core lines of Roth and Peikert missed significant parts in three cases.

The definition of Strawn, Kenwright and Ahmad did not produce applicable results in the majority of cases, which is conspicuous since it is the only definition that is solely based on vorticity. As a consequence, a combination of two different quantities in a vortex definition seems advantageous.

Vortex definitions based on pressure could only be tested on two datasets, which at the same time featured a low grid resolution. Limited to these examples, the definition of Banks and Singer produced longer true positives in contrast to Kida and Miura.

In conclusion, many vortex core lines of aneurysm datasets contained critical points which prompted the proposal of a suitable criterion. The attempt to explicitly consider critical points was not found in the literature, that addresses the *Parallel Vectors Operator*. Since the underlying application area of these publications are turbomachinery flows, critical points on core lines are perhaps more common in the field of blood flow.

5.1 Outlook

A consequence of the results is the handling of multiple valid points on a grid cell's faces. In fact, a more elaborate handling of different cases is necessary, since a cell with multiple valid points cannot be disregarded in general. This comes especially apparent for grid cells other than tetrahedrons providing more possibilities for the interpretation of the spatial flow.

Another consequence is the need of a mechanism that closes gaps in a reasonable way by connecting mutually opposite line endings below a certain distance. To not depend on a parameter respectively the scale of a dataset, the maximal distance should be automatically derived from previous steps.

The current implementation cannot handle closed core lines respectively removes a core line from the set of lines the moment it would be closed. This leads to a deletion of points whose effects are difficult to oversee and needs to be approached in a follow-up.

An alternative or addition to the post-processing could be an implementation of a geometric verification approach with the help of streamlines, as proposed by Jiang et al. [20]. It basically automates the visual inspection process by determining whether or not streamlines seeded from a core line are swirling around the core. Provided that this technique succeeds, the idea of combining different vortex definitions, as stated by Biwas et al. [3] in the context of core region, can be reassessed.

Bibliography

- [1] BANKS, D. C., AND SINGER, B. A. A predictor-corrector technique for visualizing unsteady flow. *IEEE Transactions on Visualization and Computer Graphics* 1, 2 (1995), 151–163.
- [2] BERDAHL, C. H., AND THOMPSON, D. S. Eduction of swirling structure using the velocity gradient tensor. *AIAA Journal* 31, 1 (1993), 97–103.
- [3] BISWAS, A., THOMPSON, D., HE, W., DENG, Q., CHEN, C.-M., SHENK, H.-W., MACHIRAJU, R., AND RANGARAJAN, A. An uncertainty-driven approach to vortex analysis using oracle consensus and spatial proximity. In *IEEE Pacific Visualization Symposium* (2015), pp. 223–230.
- [4] BYRNE, G. A. *Vortex-based spatiotemporal characterization of nonlinear flows*. PhD thesis, George Mason University, 2013.
- [5] BYRNE, G. A., AND CEBRAL, J. R. Vortex dynamics in cerebral aneurysms. *arXiv 1309.7875* (2013).
- [6] BYRNE, G. A., MUT, F., AND CEBRAL, J. R. Quantifying the large-scale hemodynamics of intracranial aneurysms. *American Journal of Neuroradiology* 35, 2 (2014), 333–338.
- [7] CEBRAL, J. R., MUT, F., WEIR, J., AND PUTMAN, C. M. Association of hemodynamic characteristics and cerebral aneurysm rupture. *American Journal of Neuroradiology* 32, 2 (2011), 264–270.
- [8] CHAKRABORTY, P., BALACHANDAR, S., AND ADRIAN, R. J. On the relationships between local vortex identification schemes. *Journal of Fluid Mechanics* 535 (2005), 189–214.

- [9] CHONG, M. S., PERRY, A. E., AND CANTWELL, B. J. A general classification of three-dimensional flow fields. *Physics of Fluids A: Fluid Dynamics* 2, 5 (1990), 765–777.
- [10] DA SILVA, C. B., AND PEREIRA, J. C. F. Invariants of the velocity-gradient, rate-of-strain, and rate-of-rotation tensors across the turbulent/nonturbulent interface in jets. *Physics of Fluids* 20, 5 (2008).
- [11] GASTEIGER, R. *Visual exploration of cardiovascular hemodynamics*. PhD thesis, OvGU Magdeburg, 2014.
- [12] GLOBUS, A., LEVIT, C., AND LASINSKI, T. A tool for visualizing the topology of three-dimensional vector fields. In *Proceedings of the IEEE Conference on Visualization* (1991), pp. 33–40.
- [13] GÜNTHER, T., SCHULZE, M., AND THEISEL, H. Rotation invariant vortices for flow visualization. *IEEE Transactions on Visualization and Computer Graphics* 22, 1 (2016), 817–826.
- [14] HAIMES, R., AND KENWRIGHT, D. On the velocity gradient tensor and fluid feature extraction. In *Proceedings of the 14th AIAA Computational Fluid Dynamics Conference* (1999).
- [15] HELMAN, J. L., AND HESSELINK, L. Representation and display of vector field topology in fluid flow data sets. *IEEE Computer* 22, 8 (1989), 27–36.
- [16] HUNT, J. C. R., WRAY, A. A., AND MOIN, P. Eddies, streams, and convergence zones in turbulent flows. *Proceedings of the Summer Program CTR-S88, Center for Turbulence Research, Stanford University*, 1988.
- [17] INGALL, T., ASPLUND, K., MÄHÖNEN, M., BONITA, R., ET AL. A multinational comparison of subarachnoid hemorrhage epidemiology in the WHO MONICA stroke study. *Stroke* 31, 5 (2000), 1054–1061.
- [18] JEONG, J., AND HUSSAIN, F. On the identification of a vortex. *Journal of Fluid Mechanics* 285 (1995), 69–94.
- [19] JIANG, M. *A feature-based approach to visualizing and mining simulation data*. PhD thesis, The Ohio State University, 2005.

- [20] JIANG, M., MACHIRAJU, R., AND THOMPSON, D. S. Geometric verification of swirling features in flow fields. In *Proceedings of the IEEE Conference on Visualization (2002)*, pp. 307–314.
- [21] JIANG, M., MACHIRAJU, R., AND THOMPSON, D. S. A novel approach to vortex core region detection. In *Proceedings of the Eurographics/IEEE VGTC Symposium on Visualization (2002)*, pp. 217–225.
- [22] KIDA, S., AND MIURA, H. Identification and analysis of vortical structures. *European Journal of Mechanics-B/Fluids* 17, 4 (1998), 471–488.
- [23] KIYOSUE, H., TANOUE, S., OKAHARA, M., HORI, Y., NAKAMURA, T., NAGATOMI, H., AND MORI, H. Anatomic features predictive of complete aneurysm occlusion can be determined with three-dimensional digital subtraction angiography. *American Journal of Neuroradiology* 23, 7 (2002), 1206–1213.
- [24] LEVY, Y., DEGANI, D., AND SEGNER, A. Graphical visualization of vortical flows by means of helicity. *AIAA Journal* 28, 8 (1990), 1347–1352.
- [25] LUGT, H. J. The dilemma of defining a vortex. In *Recent developments in theoretical and experimental fluid mechanics*, U. Müller, K. G. Roesner, and B. Schmidt, Eds. Springer, 1979, pp. 309–321.
- [26] OELTZE-JAFRA, S., CEBRAL, J. R., JANIGA, G., AND PREIM, B. Cluster analysis of vortical flow in simulations of cerebral aneurysm hemodynamics. *IEEE Transactions on Visualization and Computer Graphics* 22, 1 (2016), 757–766.
- [27] OKUBO, A. Horizontal dispersion of floatable particles in the vicinity of velocity singularities such as convergences. In *Deep sea research and oceanographic abstracts (1970)*, vol. 17, pp. 445–454.
- [28] PEIKERT, R., AND ROTH, M. The “parallel vectors” operator: A vector field visualization primitive. In *Proceedings of the IEEE Conference on Visualization (1999)*, pp. 263–270.
- [29] PERRY, A. E., AND CHONG, M. S. A description of eddying motions and flow patterns using critical-point concepts. *Annual Review of Fluid Mechanics* 19, 1 (1987), 125–155.

- [30] PORTELA, L. M. *Identification and characterization of vortices in the turbulent boundary layer*. PhD thesis, Stanford University, 1997.
- [31] RINKEL, G. J., DJIBUTI, M., ALGRA, A., AND VAN GIJN, J. Prevalence and risk of rupture of intracranial aneurysms: A systematic review. *Stroke* 29, 1 (1998), 251–256.
- [32] ROBINSON, S. K. Coherent motions in the turbulent boundary layer. *Annual Review of Fluid Mechanics* 23, 1 (1991), 601–639.
- [33] ROTH, M. *Automatic extraction of vortex core lines and other line-type features for scientific visualization*. PhD thesis, ETH Zürich, 2000.
- [34] ROTH, M., AND PEIKERT, R. A higher-order method for finding vortex core lines. In *Proceedings of the IEEE Conference on Visualization* (1998), pp. 143–150.
- [35] SADARJOEN, A., AND POST, F. H. Geometric methods for vortex extraction. In *Proceedings of the Eurographics/IEEE VGTC Symposium on Visualization* (1999), pp. 53–62.
- [36] SADLO, F., PEIKERT, R., AND PARKINSON, E. Vorticity based flow analysis and visualization for pelton turbine design optimization. In *Proceedings of the IEEE Conference on Visualization* (2004), pp. 179–186.
- [37] SAHNER, J. *Extraction of vortex structures in 3d flow fields*. PhD thesis, OVGU Magdeburg, 2009.
- [38] SAHNER, J., WEINKAUF, T., AND HEGE, H.-C. Galilean invariant extraction and iconic representation of vortex core lines. In *Proceedings of the Eurographics/IEEE VGTC Symposium on Visualization* (2005), pp. 151–160.
- [39] SATO, M., AND PEIKERT, R. Core-line-based vortex hulls in turbomachinery flows. *Journal of the Visualization Society of Japan* 23, 2 (2003), 151–154.
- [40] SCHROEDER, W., MARTIN, K., AND LORENSEN, B. *The Visualization Toolkit: An Object-Oriented Approach to 3D Graphics, 4th Edition*. Kitware, 2006.

- [41] STRAWN, R. C., KENWRIGHT, D. N., AND AHMAD, J. Computer visualization of vortex wake systems. *AIAA Journal* 37, 4 (1999), 511–512.
- [42] SUJUDI, D., AND HAIMES, R. Identification of swirling flow in 3D vector fields. In *Proceedings of the 12th AIAA Computational Fluid Dynamics Conference* (1995).
- [43] VLAK, M. H. M., ALGRA, A., BRANDENBURG, R., AND RINKEL, G. J. Prevalence of unruptured intracranial aneurysms, with emphasis on sex, age, comorbidity, country, and time period: a systematic review and meta-analysis. *The Lancet Neurology* 10, 7 (2011), 626–636.
- [44] VOSS, S. Untersuchung des Einflusses von Fluid-Struktur-Interaktionen auf die Hämodynamik intrakranieller Aneurysmen. Master’s thesis, OvGU Magdeburg, 2015.
- [45] WARDLAW, J. M., AND WHITE, P. M. The detection and management of unruptured intracranial aneurysms. *Brain* 123, 2 (2000), 205–221.
- [46] WEINKAUF, T. *Extraction of topological structures in 2D and 3D vector fields*. PhD thesis, OvGU Magdeburg, 2008.
- [47] WEISS, J. The dynamics of enstrophy transfer in two-dimensional hydrodynamics. *Physica D: Nonlinear Phenomena* 48, 2-3 (1991), 273–294.
- [48] XIANG, J., NATARAJAN, S. K., TREMMEL, M., MA, D., MOCCO, J., HOPKINS, L. N., SIDDIQUI, A. H., LEVY, E. I., AND MENG, H. Hemodynamic–morphologic discriminants for intracranial aneurysm rupture. *Stroke* 42, 1 (2011), 144–152.
- [49] YATES, L. A., AND CHAPMAN, G. T. Streamlines, vorticity lines, and vortices around three-dimensional bodies. *AIAA Journal* 30, 7 (1992), 1819–1826.
- [50] ZHOU, J., ADRIAN, R. J., BALACHANDAR, S., AND KENDALL, T. M. Mechanisms for generating coherent packets of hairpin vortices in channel flow. *Journal of Fluid Mechanics* 387 (1999), 353–396.